Microporous and Mesoporous Materials 360 (2023) 112713

Contents lists available at ScienceDirect

Microporous and Mesoporous Materials

journal homepage: www.elsevier.com/locate/micromeso

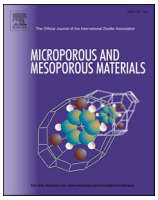

Synthesis of SAPO-34 nanocrystallites by epoxy-functional organosilane with improved MTO catalytic performance

Pengfei Wu [a,b], Dong Fan [b], Lin Liu [b], Miao Yang [b,*], Peng Tian [b,**], Zhongmin Liu [b]

[a] CAS Key Laboratory of Science and Technology on Applied Catalysis, Dalian Institute of Chemical Physics, Chinese Academy of Sciences, Dalian, 116023, China
[b] National Engineering Research Center of Lower-Carbon Catalysis Technology, Dalian National Laboratory for Clean Energy, iChEM (Collaborative Innovation Center of Chemistry for Energy Materials), Dalian Institute of Chemical Physics, Chinese Academy of Sciences, Dalian, 116023, China

ARTICLE INFO

Keywords:
SAPO molecular sieve
Nanocrystallite
Acid catalysis
Methanol-to-olefin reaction
Hydrothermal synthesis

ABSTRACT

Synergic regulation of microstructure, morphology and acidity of SAPO-34 molecular sieve is crucial to enhance its catalytic performance for methanol to olefins (MTO) reaction. Herein, a commercial oxygen-containing organosilane 3-glycidoxypropyltrimethoxysilane (AC-230) was developed as a new mesoporogen to synthesize pure SAPO-34 nanocrystallites together with diisopropylamine and seeds. According to the conditional experiments and systematic characterizations, it was disclosed that AC-230 not only changed the morphology and particle size of the SAPO-34 crystals but also affected its compositions and acidic properties. The addition of seed was indispensable to fasten the crystallization rate and hence assure the crystal growth inhibition function of AC-230. Thanks to the formed shortened diffusion pathway, moderate acid sites and pure CHA structure of the nanosized SAPO-34 product, the catalyst demonstrates excellent catalytic performance with a longer lifetime (395 min) and higher ethylene plus propylene selectivity (82.88%) in comparison to its conventional analogs (259 min and 80.63%).

1. Introduction

Silicoaluminophosphates (SAPO) molecular sieves with ordered microporous structure, tunable acidity and high (hydro)thermal stability are promising heterogeneous acid catalysts [1–3]. Among SAPOs, SAPO-34 with around 3.8 Å 8-membered ring (8-MR) pore openings and nanosized CHA cages is one of the most important members, which has attracted great attention due to its high activity and light olefins selectivity in the methanol-to-olefin (MTO) reaction [2,4,5]. The first commercial MTO unit based on SAPO-34 catalyst was implemented in 2010. Currently, more than 20 sets of MTO units have been put into operation and produced more than 16 Mt of light olefines per year. Comprehensively improving the catalytic performance of SAPO-34 catalyst has always been a research hotspot in both academia and industry fields.

Fast deactivation is a major drawback of SAPO-34 catalyst, which was caused by the unequal spatial dimension of narrow 8-MR pore openings and large CHA cavity resulting in mass transfer limitation and rapid coke deposition [5,6]. To depress the rapid deactivation issue, SAPO-34 with low silica content (acid density) is highly desirable to reduce side reactions such as aromatization and hydrogen transfer so that the coke formation rate can be decreased, and thereby prolong the catalytic lifetime [7,8]. Meanwhile, various synthetic strategies, such as dual template method [9,10], dry gel conversion method [11,12], hard-template method [13], soft-template method [14,15] and post-synthesis method [16–18] were developed to achieve SAPO-34 nanocrystallites or hierarchical SAPO-34 to shorten the diffusion distance of methanol and/or intermediates and improve the mass transfer efficiency [19]. However, the collaborative regulation of topological microstructure, morphology and acid property of SAPO-34 is still full of challenge.

Taking the most popular soft-template [3-(trimethoxysilyl)propyl] octadecyldimethylammonium chloride (TPOAC) as the example, the organosilane surfactant fabricate hierarchical SAPO-34 efficiently in various organic structure-directing agent (OSDA, e.g. triethylamine, tetraethylammonium hydroxide, diethylamine, morpholine) systems due to the strong interactions between organosiloxane groups and inorganic framework, while the hydrophobic alkyl-chain tails oriente mesopores simultaneously [20–23]. However, the hierarchical SAPO-34 product directed by tetraethylammonium hydroxide was ineffective as MTO reaction catalyst, even if it presented the smallest particle size and

* Corresponding author.
** Corresponding author.
E-mail addresses: yangmiao@dicp.ac.cn (M. Yang), tianpeng@dicp.ac.cn (P. Tian).

https://doi.org/10.1016/j.micromeso.2023.112713
Received 17 May 2023; Received in revised form 13 June 2023; Accepted 21 June 2023
Available online 22 June 2023

the most abundant mesoporous structure [24]. This is primarily because tetraethylammonium hydroxide generally directs SAPO-34 with intrinsic moderate acid sites, while the introduction of organosilane further weakens the acid strength of the catalyst, resulting in its inability to promote the MTO catalytic process. Hence, it is crucial to take into account the synergistic effect between soft template and OSDA which may determine the final MTO catalytic performance of SAPO-34 product.

In recent years, some multifunctional short-chain organosilanes, including 3-piperazinepropylmethyldimethoxysilane [25], phenylaminopropyltrimethoxysilane [26], and N-[3-(trimethoxysilyl)propyl] ethylenediamine [27] have been demonstrated to be effective for the synthesis of SAPO-34 nanocrystals in different specified OSDA systems. Note that the above mentioned organosilane molecules contain nitrogen-containing groups, which have similar chemical characteristics to the micropore templates and help enhance the intensive interactions between organosilanes and the SAPO framework. However, the existence of nitrogen-containing groups also poses the risk of introducing impure crystalline phases, which consequently narrows the crystalline phase zone, limits the regulation of the acidity and stability of catalysts. In contrast, oxygen-containing organosilanes might serve as a promising substitute without any interference from nitrogen atom. It interacts with the SAPO-34 framework via the coordination of lone pair electrons of oxygen atoms, while retains the highly active organosilane group [28,29].

In this work, a commercial low-cost organosilane, containing both epoxy-functional and organosilane groups 3-glycidoxypropyltrimethoxysilane (AC-230) was selected to synthesize SAPO-34. The pivotal synthetic parameters for achieving nanocrystallites, including AC-230/Al_2O_3 ratio, type of OSDA and the addition of seeds were firstly investigated. High-quality pure SAPO-34 nanocrystallites was achieved when diisopropylamine (DIPA) was used as an OSDA with an optimized reaction condition. Then, the resultant catalysts were well characterized, and their formation mechanism was proposed. Finally, the obtained catalysts were used for MTO reaction, obtaining elevated stability and activity due to its nanocrystallites morphology, adequate acidic properties and pure CHA structure.

2. Experimental

2.1. Synthesis

2.1.1. Chemical reagents

Orthophosphoric acid (H_3PO_4, 85 wt%), tetraethyl orthosilicate (TEOS, 98 wt%), aluminium isopropoxide ($Al(i\text{-}C_3H_7O)_3$, 99 wt%), triethylamine (TEA, 99 wt%) and diisopropylamine (DIPA, 99 wt%) were purchased from Tianjin Kemiou Chemical Reagent Company. Silica sol (31 wt%) was purchased from Shenyang Chemical Industry Co., Ltd. Pseudoboehmite (72.5 wt%) was purchased from Shandong Aluminum Industry Co., Ltd. 3-glycidoxypropyltrimethoxysilane ($CH_2OCHCH_2O(CH_2)_3Si(OCH_3)_3$, AC-230, 99 wt%) was purchased from Nanjing Aocheng Chem Co. All chemicals were used as received without further purification.

2.1.2. Preparation of milled SAPO-34 seeds

The SAPO-34 seeds were synthesized according to our previous report [30].

2.1.3. Synthesis of MSP-D and MSP-TEA

All synthesis experiments were carried out by hydrothermal method. A typical synthesis procedure was as follows: H_3PO_4 and $Al(i\text{-}C_3H_7O)_3$ were first added into deionized water and stirred for 30min. And then, the organic template R (DIPA or TEA), SAPO-34 seeds, TEOS, and AC-230 were added in sequence. The amount of the seeds was calculated by the following formula: Seeds amount (x%) = M(milled SAPO-34) × 100/M$(Al_2O_3 + P_2O_5 + SiO_2)_{gel}$ %, where milled SAPO-34 and M$(Al_2O_3 + P_2O_5 + SiO_2)_{gel}$ stand for the weights of the milled SAPO-34 and the dry mass of three inorganic oxides in the starting mixture, respectively. The mixture was stirred for 12 h and transferred into a stainless steel autoclave and heated at 200 °C for 24 h under rotation. The autoclave was cooled down and the solid product was recovered by filtration, washed three times with deionized water and dried at 110 °C overnight. Finally, the product was calcined at 600 °C for 4 h to remove organic species. The sample denoted as MSP-D and MSP-TEA corresponds to the use of organic template DIPA and TEA, respectively.

2.1.4. Synthesis of SP-D

The synthetic procedure of reference samples SP-D is the same as MSP-D except that some raw materials are omitted. The samples (SP-D3 and SP-D4) with similar silica content to MSP-D1 were synthesized by using silica sol as the Si source and pseudoboehmite as the Al source.

2.2. Characterization

The powder X-ray diffraction (XRD) patterns were recorded on a PANalytical X′ Pert PRO X-ray diffractometer with Cu-Kα radiation (λ = 1.54059 Å), operating at 40 kV and 40 mA. The bulk and surface compositions of samples were determined using a Philips Magix-601 XRF spectrometer and a Thermo ESCALAB 250Xi spectrometer (XPS) with Al Kα radiation as the excitation source. The crystal morphology was observed by scanning electron microscopy (SEM) using a field emission SEM (Hitachi SU8020). High angle annular dark field (HAADF) scanning transmission electron microscopy (STEM) images were obtained by using a JEM-2100F microscope. Textural properties of the calcined samples were measured by N_2 adsorption at −196 °C on a Micromeritics ASAP 2020 analyzer. The total surface area was calculated based on the BET equation. The micropore volume and micropore surface area were evaluated by using the t-plot method. The mesopore volume and mesopore surface area were evaluated from the adsorption isotherm by the Barrett–Joyner–Halenda (BJH) method. The temperature-programmed desorption of ammonia (NH_3-TPD) was carried out with Micromeritics Autochem II 2920 device. The calcined samples (200 mg) were outgassed in a He flow at 600 °C for 60 min. And then the samples were cooled down to 100 °C and subjected to a flow of NH_3/He for 60 min to saturate the sample with NH_3. Then, the samples were purged with a He flow to remove the weakly adsorbed NH_3 molecules. The measurement of the desorbed NH_3 was performed from 100 °C to 650 °C at a heating rate of 10 °C min^{-1} under a He flow (20 mL min^{-1}). Thermogravimetric and differential thermal analysis (TG-DTA) were performed on a TA SDTQ600 analyzer with a temperature-programmed rate of 10 °C min^{-1} in air. ^{13}C magic-angle-spinning (MAS) and ^{29}Si cross-polarization (CP) nuclear magnetic resonance (NMR) were carried out on a Bruker AvanceIII 600 spectrometer at 150.9 MHz for ^{13}C and 119.2 MHz for ^{29}Si. ^{13}C MAS NMR spectra were recorded with a 4 mm MAS probe with a spinning rate of 12 kHz. ^{29}Si CP NMR spectra were measured with a contact time of 3 ms and a recycle delay of 2 s ^{29}Si CP NMR spectra were recorded with a 4 mm MAS probe with a spinning rate of 8 kHz. Chemical shifts were referenced to adamantane for ^{13}C and 4,4-dimethyl-4-silapentane sulfonate sodium salt (DSS) for ^{29}Si.

2.3. Catalytic test and qualitative analysis of coke deposits

MTO reaction was performed in a quartz tubular fixed-bed reactor at atmospheric pressure. 0.30 g calcined catalyst (40–60 mesh) was loaded in the quartz reactor and activated at 550 °C in a N_2 flow of 30 mL min^{-1} for 1 h before starting each reaction run, subsequently the temperature was adjusted to a reaction temperature of 450 °C. The methanol was fed by passing the carrier gas (28 mL min^{-1}) through a saturator containing methanol at 30 °C, which gave a weight hourly space velocity (WHSV) of 2 h^{-1}. The reaction products were analyzed using an online gas chromatograph (Agilent GC 7890 N), equipped with a flame ionization detector (FID) and Plot-Q column. The amount of generated coke on

Table 1
Synthesis conditions and resultant products of hydrothermal synthesis.

Sample	Gel composition				Product	Product size	Product composition	
	R	TEOS	AC-230	Seeds			Bulk (XRF)	Surface (XPS)
SP-D1[a]	DIPA	0	0.4	-	$AlPO_4$-11	-	-	
SP-D2[a]	DIPA	0.3	0.3	-	SAPO-34	5 μm	$Si_{0.092}Al_{0.494}P_{0.414}O_2$	
SP-D3[b]	DIPA	0.45	0	-	SAPO-34	5 μm	$Si_{0.097}Al_{0.489}P_{0.413}O_2$	
SP-D4[b]	DIPA	0.45	0	2%	SAPO-34	2 μm	$Si_{0.096}Al_{0.492}P_{0.412}O_2$	
MSP-D1[a]	DIPA	0.3	0.15	2%	SAPO-34	250–300 nm	$Si_{0.092}Al_{0.545}P_{0.363}O_2$	$Si_{0.098}Al_{0.467}P_{0.434}O_2$
MSP-D2[a]	DIPA	0.3	0.3	2%	SAPO-34	250–300 nm	$Si_{0.094}Al_{0.182}P_{0.465}O_2$	
MSP-D3[a]	DIPA	0.3	0.45	2%	SAPO-34	200–250 nm	$Si_{0.107}Al_{0.483}P_{0.410}O_2$	
MSP-TEA[c]	TEA	0.32	0.1	2%	SAPO-34/18	350 nm	$Si_{0.088}Al_{0.542}P_{0.371}O_2$	$Si_{0.084}Al_{0.499}P_{0.471}O_2$

[a] Initial gel molar composition: $DIPA/Al_2O_3/P_2O_5/TEOS/AC\text{-}230/H_2O = 3.5/1.0/1.0/x/y/100$.
[b] For SP-D3 and SP-D4, pseudoboehmite and silica sol are used as the Al source and Si source, respectively. Initial gel molar composition: $DIPA/Al_2O_3/P_2O_5/SiO_2/H_2O = 3.0/1.2/0.9/0.45/40$.
[c] Initial gel molar composition: $TEA/Al_2O_3/P_2O_5/TEOS/AC\text{-}230/H_2O = 4.5/1.0/1.0/0.32/0.1/100$.

Table 2
Textural properties of the samples.

Sample	Surface area (m^2/g)			Pore volume (cm^3/g)	
	S_{total}[a]	S_{micro}[b]	S_{exter}[b]	V_{micro}[b]	V_{meso}[c]
SP-D3	564	561	3	0.28	0.00
SP-D4	570	561	9	0.28	0.01
MSP-D1	604	539	65	0.26	0.31
MSP-D2	566	512	51	0.25	0.18
MSP-D3	615	520	95	0.26	0.30
MSP-TEA	596	515	81	0.25	0.19

[a] Total surface area is determined by the BET equation.
[b] Micropore surface area, micropore volume and external surface area are determined by the t-plot method.
[c] Mesopore volume is determined from the adsorption isotherm by the BJH method.

catalysts after the MTO reaction was determined by thermal analysis on a TA SDTQ600 analyzer at a heating rate of 10 °C min^{-1} from room temperature to 900 °C under air flow.

In order to capture the organic intermediates confined in the catalysts, the MTO reaction was operated as follow. After methanol feeding for 40 min at 350 °C, the catalyst sample which had 100% methanol conversion at this stage was removed from the reactor quickly and put into liquid nitrogen to prevent the active intermediates from further reaction. The retained compounds in the catalysts were extracted by HF and analyzed by GS-MS.

The Guisnet method was used for the qualitative analysis of the coke species [31]. In a Teflon bottle, 100 mg catalyst was added into 2 mL HF solution (20 wt %). After the mixture was still standing for 1.5 h, 1 mL dichloromethane was added into the solution to extract coke species. NaOH solution (5 wt %) was added to neutralize HF. The organic phase was collected and analyzed by GC-MS testing with a HP-5 capillary column. Each compound was identified using the NIST11 database.

3. Results and discussion

3.1. Synthesis and characterization

A series of SAPO samples were prepared by introducing organosilane AC-230 into the DIPA template system. If necessary, small amount of milled SAPO-34 seeds was added to modify the crystallization process. Detailed synthetic conditions, resultant XRD and SEM results are listed in Table 1, Figs. 1 and 2.

When AC-230 was used as the only silica source, the silica-free $AlPO_4$-11 (SP-D1) was the final product. When TEOS was coexistence with AC-230, bulky cubic SAPO-34 (SP-D2, Fig. 2a) was obtained with a particle size similar to that of the conventional reference sample (SP-D3, Fig. 2b). The above phenomena show that AC-230, as the only silica source cannot participate in SAPO-34 crystallization process effectively. Interestingly, the morphology of SAPO-34 products (MSP-D1~D3) change to very small nano crystals (below 300 nm) with rough surface when a small amount of seeds was added with a $TEOS/Al_2O_3$ ratio of higher than 0.3. Keeping the dosage of TEOS constant, the crystal size of the samples shows a decrease with the increased usage of AC-230, implying that AC-230 can restrain the growth of the SAPO-34 crystals under the assistance of seeds. As shown in Fig. 2d, MSP-D1 presented the cubic morphology with quite rough surface, whose particle size was about 250–300 nm. Meanwhile, it is obvious that some visible mesopores randomly located inside the SAPO-34 crystals (Fig. 2e). Both MSP-D2 (Fig. 2f) and MSP-D3 (Fig. 2g) showed similar nanocrystalline morphology, with slightly decreased particle sizes ranged from 150 to

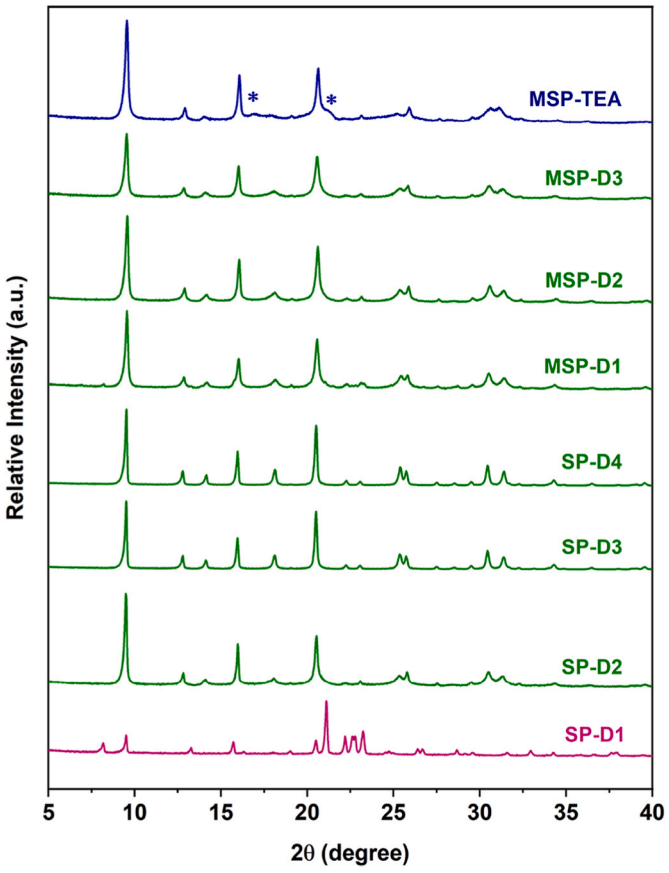

Fig. 1. XRD patterns of the as-synthesized samples. Asterisks indicate the AEI phase.

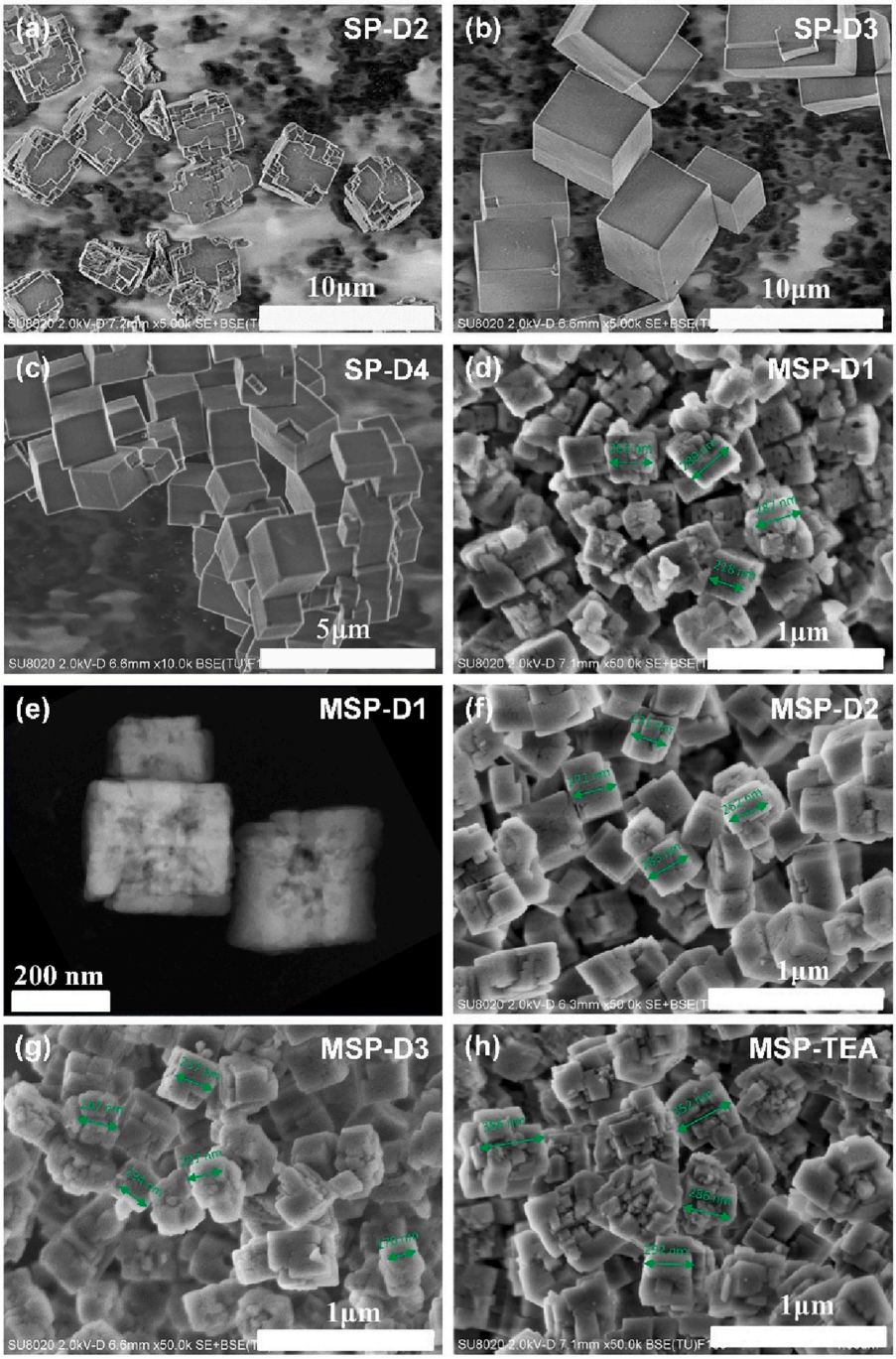

Fig. 2. SEM images of calcined SP-D2 (a), SP-D3 (b), SP-D4 (c), MSP-D1 (d), MSP-D2 (f), MSP-D3 (g), MSP-TEA (h), and HAADF-STEM image of calcined MSP-D1 (e).

300 nm. In addition, XRF analysis shows a notable increase in product Si content from MSP-D1 to MSP-D3, which evidences the incorporation of organosiloxane group into the SAPO-34 product. Notably, our experimental results revealed that the particle size of the DIPA-directed sample remained nearly unaltered even if a high amount of AC-230 was used. It is speculated that the capability of the organosilane to engage in crystallization has a certain maximum in DIPA system. It should be mentioned that the SAPO-34 product is 2 μm rhombic crystal with smooth surface when AC-230 is absent (SP-D4, Fig. 2c). The above comparative experiments illustrate that the co-existence of AC-230 and the seeds in the initial gel is crucial for the formation of SAPO-34 nanocrystallites.

Comparatively, when TEA was utilized as an OSDA, well-crystallized nanocrystals (MSP-TEA) with comparable silica content of MSP-D1 could also be obtained when TEOS and AC-230 were simultaneously used as silica sources together with the assistant of the seeds. Consistent with previous reports, the XRD patterns of the TEA-directed sample display two weak diffraction peaks at 16.9° and 21.3° besides those of SAPO-34, indicating the presence of SAPO-34(CHA)/18(AEI) intergrowth phase [12,32]. Although the window dimension of AEI cages is very close to that of CHA cages, the production distribution and generated coke species in the MTO reaction may differ notably due to the spatial confinement effect [33]. As seen in Fig. 2h, the low-silica MSP-TEA has an intergrowth morphology of nanocrystallites with secondary particle sizes of ca. 350 nm. According to the above results, it can be inferred that the introduction of AC-230, seed and the type of

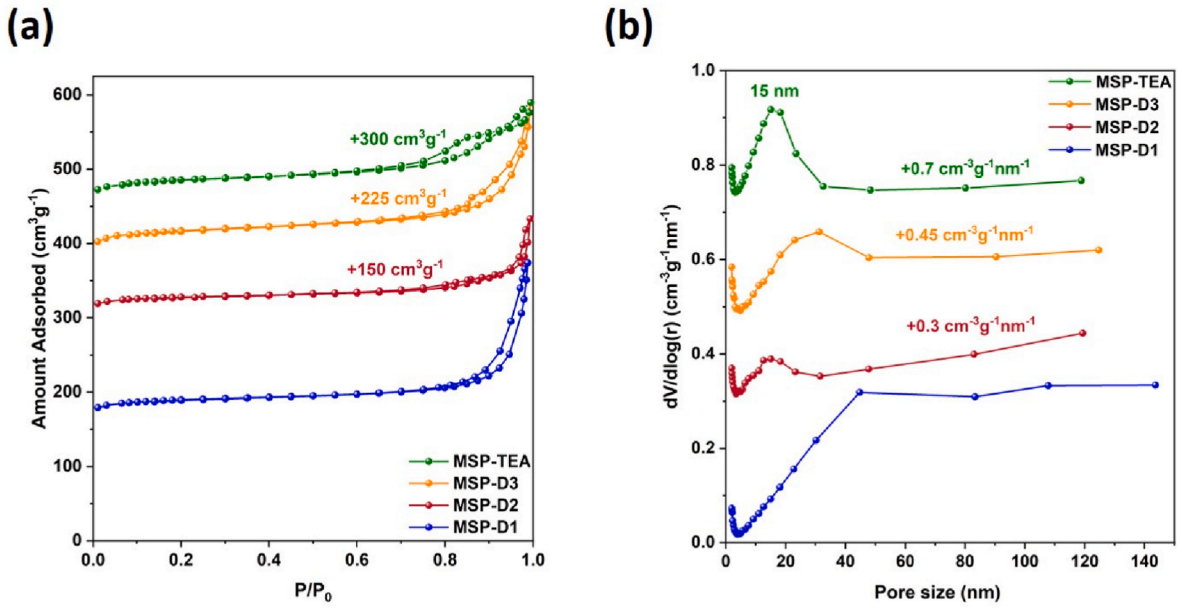

Fig. 3. N_2 sorption isotherms (a) and pore size distributions (b) of the samples.

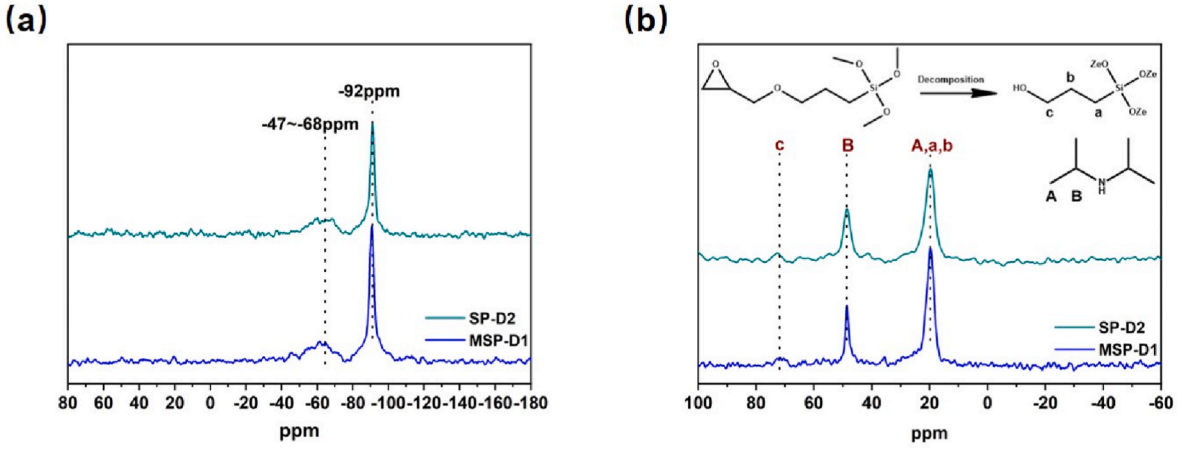

Fig. 4. ^{29}Si CP MAS NMR spectra (a) and ^{13}C MAS NMR spectra of the as-synthesized samples.

template have significant impact on the crystallization process.

The XPS results of the low-silica nanosized samples are given in Table 1. It can be seen that the samples have homogeneous Si distribution from crystal center to surface regardless of the type of OSDA, which implies the homogeneous incorporation of AC-230 in the framework and would be conducive to their MTO catalytic performance [4].

N_2 adsorption isotherms and pore size distribution of the samples are depicted in Fig. 3 and the corresponding texture results are given in Table 2. All the synthesized samples exhibit large micropore surface area of above 500 m^2/g and micropore volume of 0.25–0.28 cm^3/g, which verify their high crystallinity. In Fig. 3a, the adsorption–desorption isotherms of the nanocrystallites show a manifest increase with a hysteresis loop after $P/P_0 > 0.7$, ascribing to multilayer adsorption in the void space of nanoparticles. In comparison with the micrometer-sized analog, MSP-Ds and MSP-TEA display apparently large external surface area (51–81 m^2/g) and high mesopore volume (0.18–0.31 cm^3/g). As illustrated in Fig. 3b, MSP-Ds has a wide pore distribution, while the numerous mesopores of the MSP-TEA are centered at 15 nm. Combined with their low Si content, the catalyst MSP-D1 and MSP-TEA could provide abundant available moderate acid sites and more space for diffusion in MTO catalytic reactions.

3.2. The status of organosilane in the SAPO-34 crystals

The samples synthesized in DIPA system (SP-D2 and MSP-D1) were chosen for solid-state ^{29}Si and ^{13}C NMR investigation to learn the Si atomic environments and the status of organosilane in the products. The ^{29}Si CP MAS NMR spectra are shown in Fig. 4a. The dominant peak centered at −92 ppm is ascribed to the isolated framework $Si(OAl)_4$ species. No signals between −95 and −109 ppm arising from $Si(OAl)_n$ (n = 0, 1, 2 and 3) species in the framework can be detected, consistent with the low-silica characteristic of the samples [34]. The broad resonance from −47 to −68 ppm could be attributed to the Tn groups (Tn = $RSi(OAl)_n(OH)_{3-n}$, n = 2 and 3). It suggests that the organosiloxane groups have been condensed into the SAPO-34 framework [25]. The ^{13}C MAS NMR spectra present two strong peaks at 19.6 and 48.6 ppm corresponding to the methylene and methyl groups of DIPA undoubtedly (Fig. 4b). However, the peak area ratios of the two signals are determined to be 2.4 and 3.3 for SP-D2 and MSP-D1 respectively, which are much larger than the theoretical value of DIPA (2.0) [35]. It is speculated that the existence of organosilane contributes to the peak at 19.6 ppm. In addition, the weak resonance at around 71.5 ppm can be assigned to the primary carbon atoms connecting to hydroxyl group.

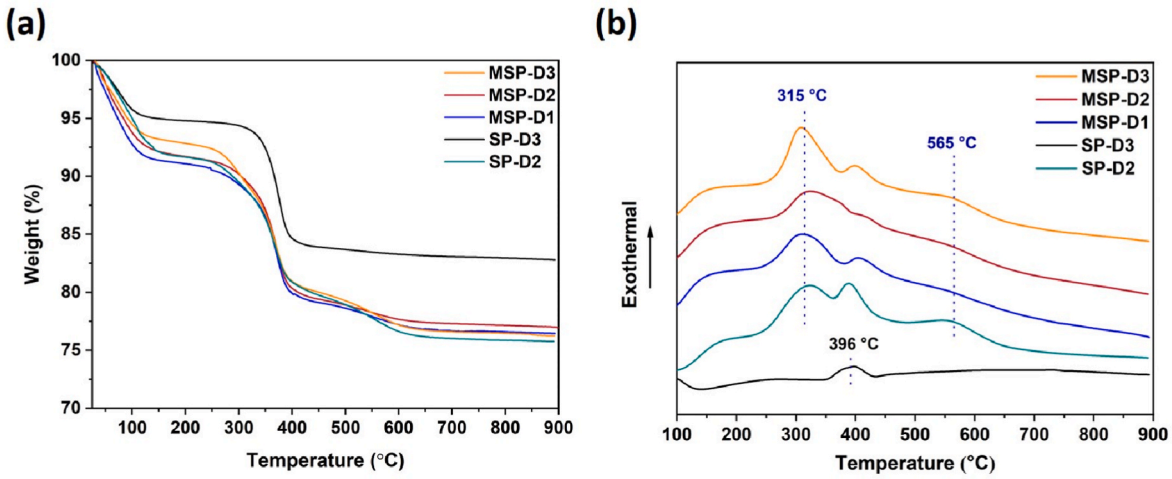

Fig. 5. TG (a) and DTA (b) curves of the as-synthesized samples.

Table 3
Thermal analysis results of the samples.

Sample	Weight loss (%)	
	Physical absorbed water (RT-200 °C)	Organic species (200–900 °C)
SP-D2	11.0	20.9
SP-D3	6.2	14.5
MSP-D1	11.6	19.2
MSP-D2	10.8	19.3
MSP-D3	9.4	21.7

These results imply that the tails of AC-230 have hydrolyzed during the crystallization process (inset of Fig. 4b), and the residual part connects to the SAPO framework to form $O_{Zeolite}$-SiPrOH structure. As the Si and C environments of SP-D2 and MSP-D1 are analogous, the addition of seeds in the gel system is supposed to have less effect on the incorporation of organosiloxane.

TG-DTA measurements were conducted to evaluate the organics in the samples (Fig. 5). The conventional SP-D3 showed just one exothermic peak centered at 396 °C in the DTA curve corresponding to the combustion of DIPA molecules encapsulated in CHA cages. The SAPO-34s synthesized with AC-230 exhibited additional broader exothermic signals at around 315 °C and 565 °C, ascribed to the removal of the organic species of the organosilane. From Table 3, the total organic weight losses of MSP-D1, MSP-D2 and MSP-D3 increased progressively and ranged from 19.2 wt% to 21.7 wt%, which are substantially higher than that of SP-D3 (14.5 wt%). Additionally, according to the organic weight losses, it is clear that the introduced amount of organosilane rises with the increase of gel AC-230/Al_2O_3 ratio. Such variation is consistent with the change of XRF results.

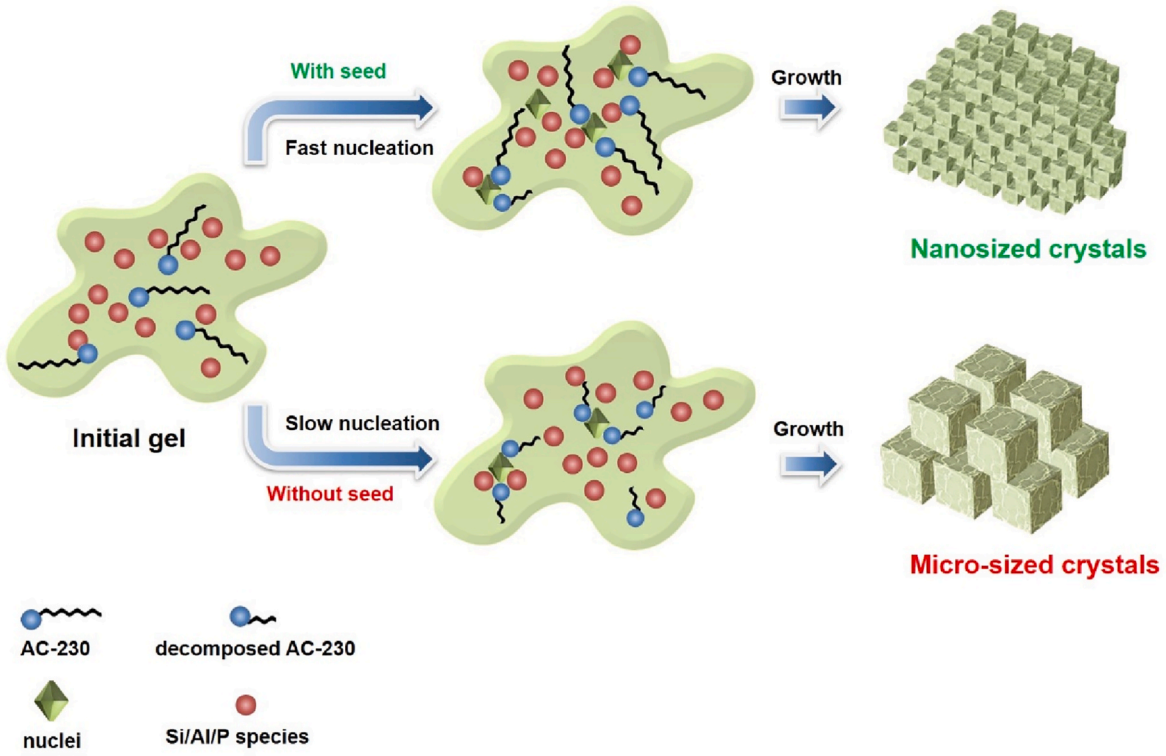

Scheme 1. The proposed crystallization process of nanosized MSP-D1 and micro-sized SP-D2. The micropore template is omitted for clarity.

Table 4
Catalytic lifetime[a] and product distribution[b] of the samples in the MTO reaction. (WHSV = 2 h^{-1}, T = 450 °C).

Sample	Lifetime (min)	$C2^=$ (%)	$C3^=$ (%)	$C2^=+C3^=$ (%)	$C4^=$ (%)	Coke content[c] (%, g $gcat^{-1}$)	R_{coke}[c] (mg min^{-1})
MSP-D1	395	50.92	31.96	82.88	8.29	28.28	0.071
SP-D3	259	48.33	32.67	81.00	8.26	23.62	0.091
MSP-TEA	327	47.43	33.20	80.63	9.11	27.73	0.084

[a] Catalyst lifetime is defined as the reaction duration with >99% methanol conversion.
[b] Based on the highest selectivity of ethene and propene under >99% methanol conversion.
[c] Determined using a TG-DTA analyzer up to 900 °C measured after the MTO reaction.

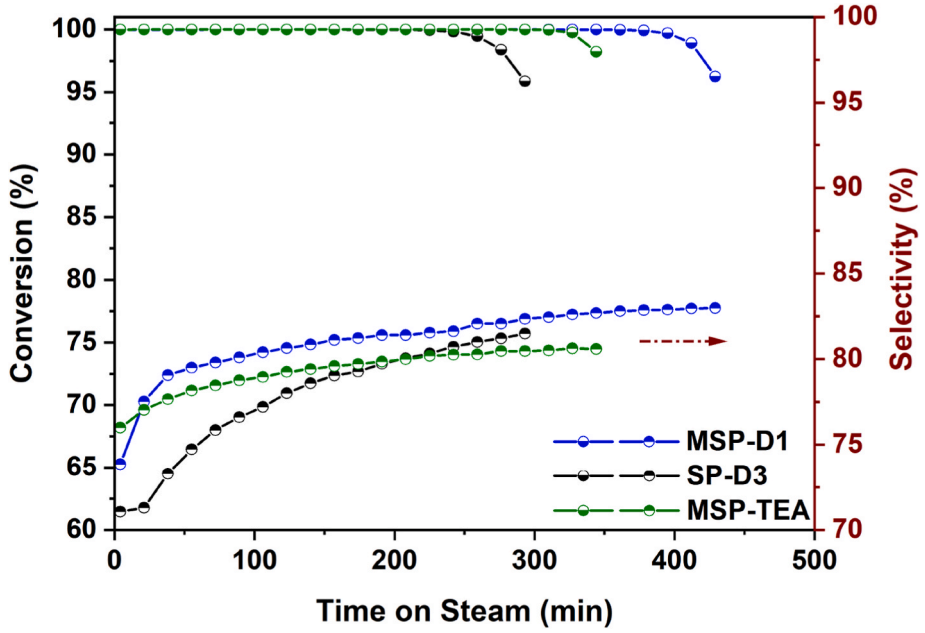

Fig. 6. Methanol conversion and (C_2H_4+C_3H_6) selectivity variation with time-on-stream over samples. Experimental conditions: WHSV = 2 h^{-1}, T = 450 °C, catalyst weight = 0.30 g.

3.3. Formation mechanism of SAPO-34 nanocrystallites

Based on these conditional experiments, AC-230 played a non-substitutable role in the formation of nanocrystallites, though it decomposed during the crystallization. A little amount of seeds, on the other hand, was also essential as they ensured the functionality of the organosilane. Based on the experimental results and analyses, the formation mechanisms of nanosized MSP-D1 and micro-sized SP-D2 are proposed and depicted in Scheme 1. Typically, the hydrothermal synthesis of molecular sieves involves two steps: I) The induction period, which is the process of assembling preliminary building units from supersaturated gels to form the nuclei, normally takes a considerable time when organosilane exists in the system; II) the crystal growth period, referring to the rapid polymerization of nutritive material on the nuclei to form the massive ordered crystal. Under the assistance of the seeds, the induction period was dramatically shortened, and more nuclei appear in a short time. The oxygen-containing groups such as epoxy group, ether group and silanol group strengthened the interactions between the organosilane and nuclei surface, while the hydrophilic tail of AC-230 hindered crystal growth, favoring the formation of SAPO-34 nanocrystallites. Otherwise, when the seeds were absent, the metastable organosiloxane would degrade completely to γ-hydroxypropyltrihydroxysilane during the longer induction period. Due to the limited size of the hydroxypropyl group, the residual organosilane was confined in CHA cage during the subsequent crystal growth stage, which was helpless for the modification of the crystal sizes though it can participant in the framework formation of SAPO-34 as part of silica source.

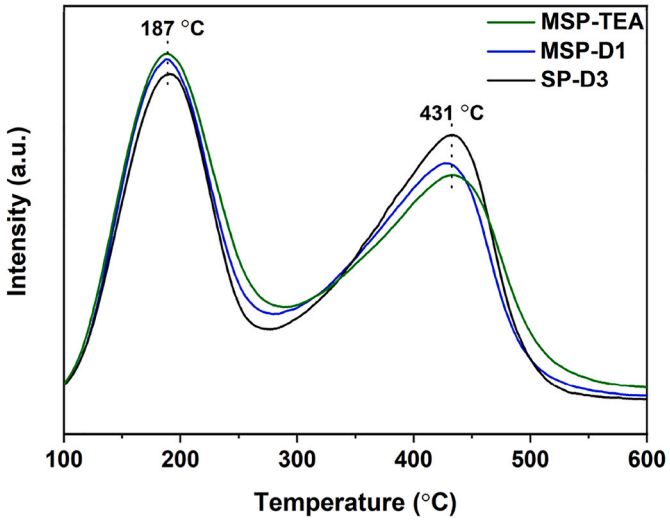

Fig. 7. NH_3-TPD profiles of the samples.

3.4. Catalytic test

As a classical acid-catalyzed nanocage-confined reaction, the MTO reaction was performed at 450 °C with a methanol WHSV of 2 h^{-1} to evaluate the catalytic performance of the samples with relatively low and comparable Si content. The catalytic results are summarized in Table 4 and Fig. 6. The nanosized MSP-D1 exhibited obviously

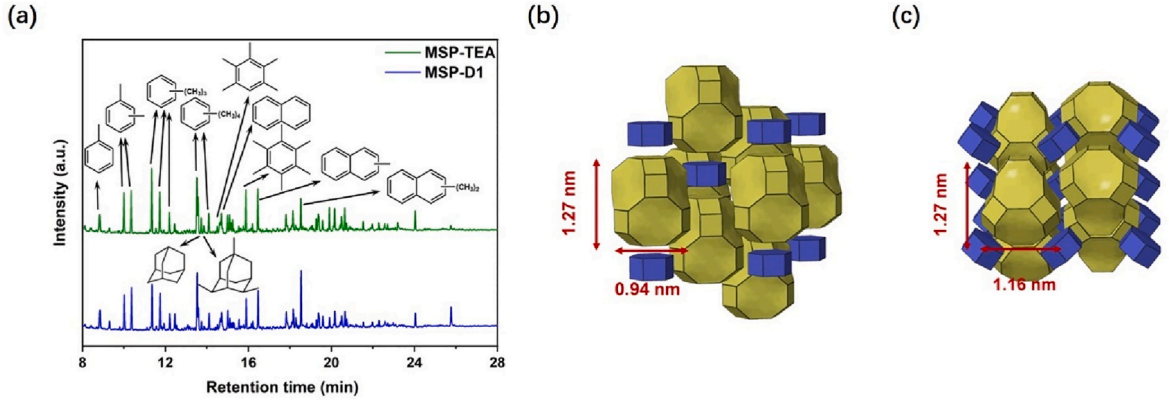

Fig. 8. GC-MS chromatograms (a) of the hydrocarbon compounds retained in MSP-D1 and MSP-TEA after the MTO reaction. Experimental condition: WHSV = 2 h^{-1}, T = 350 °C, reaction time = 40min, catalyst weight = 300 mg. Cage structure of SAPO-34 (b) and SAPO-18 (c).

Table 5
Methylbenzenes distribution[a] of samples in the MTO reaction. (WHSV = 2 h^{-1}, T = 350 °C, reaction time = 40min).

Sample	toluene (%)	xylene (%)	tri- (%)	tetra- (%)	penta- (%)	hexa- (%)	higher-substituted methylbenzenes[b] (%)
MSP-D1	7.7	23.7	33.0	26.2	3.6	5.8	9.4
MSP-TEA	6.8	22.7	31.1	24.1	8.4	6.8	15.2

[a] Only methylbenzenes species are calculated and normalized to 100% in order to make a better comparison.
[b] The summary of the proportion of penta- and hexamethylbenzene.

prolonged catalytic lifetime (395 min), higher ethene plus propene selectivity (82.88%) and slower coke formation rate (0.071 mg min^{-1}) than conventional micrometer-sized catalyst SP-D3 (259 min, 81.00% and 0.091 mg min^{-1}). The reduced crystal size of MSP-D1 should be favorable for the enhancement of mass transfer and the utilization of acid sites, leading to its superior catalytic performance. In contrast, notwithstanding MSP-TEA processed rich porosity, it showed an unsatisfactory lifespan (327 min) and selectivity to light olefins (80.62%). After excluding the influences of mass transfer limitation, the acidity and active intermediates analyses were conducted to investigate the above aberrant phenomenon.

As seen from the NH_3-TPD results (Fig. 7), although the Si contents of all catalysts are comparable, the samples displayed similar acid strength whereas the acid concentration of the AC-230 directed MSP-D1 was lower than that of SP-D3. This is in accordance with previous studies that the introduction of organosilane reduces the acid concentration of the catalyst, which has been demonstrated to possess better catalytic performance in the MTO reaction [21,23,27]. Meanwhile, MSP-TEA processed the lowest acid density. This most likely result from the organosilane weakening the acidic strength of the relatively moderate intrinsic acid sites distributed in the SAPO-18 intergrowth phase, which made them insufficient to catalyze the MTO reaction. Thus, it is supposed that the decline in stability of MSP-TEA was attributed to the excessively low active site density, leading to the rapid formation of heavy coke species [7,36,37].

Analysis of the organic intermediates retained in the nanosized MSP-D1 and MSP-TEA was further supplemented to explore the impact of cage structure on product selectivity. The experiment was conducted at 350 °C to capture the highly active intermediate species. The GC-MS results (Fig. 8a) show that hydrocarbons such as polymethylbenzenes, polymethylnaphthalenes and adamantanes are dominant in both catalysts. According to the well-recognized hydrocarbon pool mechanism, the formations of polymethylbenzenes significantly influence the olefin product distribution, and their relative distribution was summarized in Table 5. The apparent difference of the confined highly substituted methylbenzenes (penta-methylbenzene and hexa-methylbenzene) was correlated well with the subtle cage structure variation, which are 9.4% and 15.2% in MSP-D1 and MSP-TEA respectively. As seen in Fig. 8b and c, the CHA and AEI cages possess identical 8-ring pore openings of 0.38 × 0.38 nm, while the internal dimension of the pear-like AEI cage (1.27 nm × 1.16 nm) is larger than that of CHA cage (1.27 nm × 0.94 nm). It is thus speculated that the higher selectivity of propene and butene and lower selectivity of ethylene of MSP-TEA eventually resulted from the favored accommodation of highly substituted methylbenzenes in the large-size cages of SAPO-18 intergrowth phase [38,39]. Overall, it is concluded that both mass transfer property, acidity and crystalline phase are all critical for designing catalysts with superior MTO catalytic performance.

4. Conclusion

In summary, by using commercial organosilane AC-230 together with seeds and DIPA OSDA, pure SAPO-34 nanocrystallites have been successfully synthesized under rational condition. The addition of the seeds in the initial gel has been revealed to be crucial for AC-230 to play its role as crystal growth inhibiter. Otherwise, AC-230 decomposed during the long induction period and lost its effect on inhibiting the crystal growth. The SAPO-34 nanocrystallites exhibited remarkable MTO catalytic performance due to the combined contribution of small particle size, moderate acidity and pure CHA crystalline phase. It is expected that the present understanding on the matching of the stability period of organosilane and crystallization rate would facilitate the strategy development for the synthesis of hierarchical/nanosized molecular sieves.

CRediT authorship contribution statement

Pengfei Wu: Writing – original draft, Investigation, Data curation, Methodology. **Dong Fan:** Data curation. **Lin Liu:** Data curation. **Miao Yang:** Writing – review & editing, Investigation, Funding acquisition. **Peng Tian:** Writing – review & editing, Project administration, Methodology. **Zhongmin Liu:** Project administration, Funding acquisition.

Declaration of competing interest

The authors declare that they have no known competing financial

interests or personal relationships that could have appeared to influence the work reported in this paper.

Data availability

No data was used for the research described in the article.

Acknowledgment

The authors acknowledge the National Natural Science Foundation of China (No. 22108274, 21991090, 21991091, 22171259 and 52276191), the National Key R&D Projects of Ministry, Science and Technology of the People's Republic of China (Grant No. 2022YFC2105800) and the Key Research Program of Frontier Sciences, Chinese Academy of Sciences (Grant No. QYZDBSSW-JSC040).

References

[1] M.E. Potter, Down the microporous rabbit hole of silicoaluminophosphates: recent developments on synthesis, characterization, and catalytic applications, ACS Catal. 10 (2020) 9758–9789.
[2] P. Tian, Y.X. Wei, M. Ye, Z.M. Liu, Methanol to olefins (MTO): from fundamentals to commercialization, ACS Catal. 5 (2015) 1922–1938.
[3] S. Mohan, P. Dinesha, S. Kumar, NOx reduction behaviour in copper zeolite catalysts for ammonia SCR systems: a review, Chem. Eng. J. 384 (2020) 123253–123262.
[4] M. Yang, D. Fan, Y. Wei, P. Tian, Z. Liu, Recent progress in methanol-to-olefins (MTO) catalysts, Adv. Mater. 31 (2019) 1902181–1902195.
[5] Q. Sun, Z. Xie, J. Yu, The state-of-the-art synthetic strategies for SAPO-34 zeolite catalysts in methanol-to-olefin conversion, Natl. Sci. Rev. 5 (2018) 542–558.
[6] W. Yu, X. Wu, B. Cheng, T. Tao, X. Min, R. Mi, Z. Huang, M. Fang, Y. Liu, Synthesis and applications of SAPO-34 molecular sieves, Chemistry (2021), e202102787.
[7] B. Gao, M. Yang, Y. Qiao, J. Li, X. Xiang, P. Wu, Y. Wei, S. Xu, P. Tian, Z. Liu, A low-temperature approach to synthesize low-silica SAPO-34 nanocrystals and their application in the methanol-to-olefins (MTO) reaction, Catal. Sci. Technol. 6 (2016) 7569–7578.
[8] W. Dai, G. Cao, L. Yang, G. Wu, M. Dyballa, M. Hunger, N. Guan, L. Li, Insights into the catalytic cycle and activity of methanol-to-olefin conversion over low-silica AlPO-34 zeolites with controllable Brønsted acid density, Catal. Sci. Technol. 7 (2017) 607–618.
[9] L. Guo, W.P. Zhu, P. Miao, F. Li, Z.H. Guo, Q. Sun, Intergrowth silicoaluminophosphate molecular sieves synthesized and their catalytic performances for methanol to olefins reaction, Ind. Eng. Chem. Res. 57 (2018) 10398–10402.
[10] D. Zhao, Y. Zhang, Z. Li, Y. Wang, J. Yu, Synthesis of AEI/CHA intergrowth zeolites by dual templates and their catalytic performance for dimethyl ether to olefins, Chem. Eng. J. 323 (2017) 295–303.
[11] Y. Liang, B. Gao, L. Zhou, X. Yang, T. Lu, H. Yao, Y. Su, Rational construction of hierarchical SAPO-34 with enhanced MTO performance without an additional meso/macropore template, J. Mater. Chem. 9 (2021) 1859–1867.
[12] Z.H. Li, Y.S. Liu, T. Dou, X.F. Li, C.Y. Di, S.L. Chen, Sustainable synthesis of AEI/CHA intergrowth zeolites for methanol-to-olefins conversion, Microporous Mesoporous Mater. 344 (2022) 112201–112211.
[13] A.Z. Varzaneh, J. Towfighi, S. Sahebdelfar, Carbon nanotube templated synthesis of metal containing hierarchical SAPO-34 catalysts: impact of the preparation method and metal avidities in the MTO reaction, Microporous Mesoporous Mater. 236 (2016) 1–12.
[14] S. Zhang, Z. Wen, L. Yang, C. Duan, X. Lu, Y. Song, Q. Ge, Y. Fang, Controllable synthesis of hierarchical porous petal-shaped SAPO-34 zeolite with excellent DTO performance, Microporous Mesoporous Mater. 274 (2019) 220–226.
[15] G. Guo, Q. Sun, N. Wang, R. Bai, J. Yu, Cost-effective synthesis of hierarchical SAPO-34 zeolites with abundant intracrystalline mesopores and excellent MTO performance, Chem. Commun. 54 (2018) 3697–3700.
[16] S. Tao, X. Zhang, X. Li, Y. Wang, B. Wang, Y. Yuan, D. Zhang, S. Du, X. Li, Hierarchical low-silica SAPO-34 with enhanced MTO performance: mesopore template- and fluoride-free synthesis, Microporous Mesoporous Mater. 349 (2023).
[17] D. Verboekend, M. Milina, J. Pérez-Ramírez, Hierarchical silicoaluminophosphates by postsynthetic modification: influence of topology, composition, and silicon distribution, Chem. Mater. 26 (2014) 4552–4562.
[18] Y.L. Zhu, H.W. Dai, Y. Duan, Q. Chen, M. Zhang, Excellent methanol to olefin performance of SAPO-34 crystal deriving from the mixed micropore, mesopore, and macropore architecture, Cryst. Growth Des. 20 (2020) 2623–2631.
[19] K.Y. Lee, H.-J. Chae, S.-Y. Jeong, G. Seo, Effect of crystallite size of SAPO-34 catalysts on their induction period and deactivation in methanol-to-olefin reactions, Appl. Catal., A 369 (2009) 60–66.
[20] M. Choi, H.S. Cho, R. Srivastava, C. Venkatesan, D.H. Choi, R. Ryoo, Amphiphilic organosilane-directed synthesis of crystalline zeolite with tunable mesoporosity, Nat. Mater. 5 (2006) 718–723.
[21] Q. Sun, N. Wang, D. Xi, M. Yang, J. Yu, Organosilane surfactant-directed synthesis of hierarchical porous SAPO-34 catalysts with excellent MTO performance, Chem. Commun. 50 (2014) 6502–6505.
[22] L. Zhang, H. Liu, Y. Yue, U. Olsbye, X. Bao, Design and in situ synthesis of hierarchical SAPO-34@kaolin composites as catalysts for methanol to olefins, Catal. Sci. Technol. 9 (2019) 6438–6451.
[23] C. Wang, M. Yang, P. Tian, S.T. Xu, Y. Yang, D.H. Wang, Y.Y. Yuan, Z.M. Liu, Dual template-directed synthesis of SAPO-34 nanosheet assemblies with improved stability in the methanol to olefins reaction, J. Mater. Chem. 3 (2015) 5608–5616.
[24] L. Chen, R.W. Wang, S.A. Ding, B.B. Liu, H. Xia, Z.T. Zhang, S.L. Qiu, Synthesis and characterization of SAPO-34-H(hierarchical), Chemical Journal of Chinese Universities-Chinese 31 (2010) 1693–1696.
[25] P. Wu, M. Yang, W. Zhang, S. Xu, P. Guo, P. Tian, Z. Liu, Synthesis of SAPO-34 nanoaggregates with the assistance of an inexpensive three-in-one non-surfactant organosilane, Chem. Commun. 53 (2017) 4985–4988.
[26] B. Yang, P. Zhao, J. Ma, R. Li, Synthesis of hierarchical SAPO-34 nanocrystals with improved catalytic performance for methanol to olefins, Chem. Phys. Lett. 665 (2016) 59–63.
[27] C. Sun, A. Zhao, Y. Wang, Z. Wang, J. Zhao, T. Zhao, W. Liu, M. Shi, J. Lu, S. Wu, L. Bu, Organosilane-assistant synthesis of hierarchical SAPO-34 aggregates with superior MTO performance, Microporous Mesoporous Mater. 310 (2021) 110619–110627.
[28] P.F. Wu, M. Yang, J.F. Pang, D. Fan, L. Song, T.T. Sun, M.Y. Zheng, P. Tian, T. Zhang, Facile synthesis of SAPO-34 nanocrystallites with excellent performance for the dehydration of carbohydrates to 5-hydroxymethylfurfural, Green Chem. 25 (2023) 1395–1405.
[29] C. Zhang, X. Lu, T. Wang, Synthesis of SAPO-34 using metakaolin in the presence of β-cyclodextrin, J. Energy Chem. 24 (2015) 401–406.
[30] M. Yang, P. Tian, C. Wang, Y. Yuan, Y. Yang, S. Xu, Y. He, Z. Liu, A top-down approach to prepare silicoaluminophosphate molecular sieve nanocrystals with improved catalytic activity, Chem. Commun. 50 (2014) 1845–1847.
[31] M. Guisnet, P. Magnoux, Coking and deactivation of zeolites, Appl. Catal. 54 (1989) 1–27.
[32] B. Shen, X. Chen, X. Fan, H. Xiong, H. Wang, W. Qian, Y. Wang, F. Wei, Resolving atomic SAPO-34/18 intergrowth architectures for methanol conversion by identifying light atoms and bonds, Nat. Commun. 12 (2021).
[33] J.R. Chen, J.Z. Li, Y.X. Wei, C.Y. Yuan, B. Li, S.T. Xu, Y. Zhou, J.B. Wang, M. Z. Zhang, Z.M. Liu, Spatial confinement effects of cage-type SAPO molecular sieves on product distribution and coke formation in methanol-to-olefin reaction, Catal. Commun. 46 (2014) 36–40.
[34] C. Dorémieux-Morin, C. Martin, J.-M. Brégeault, J. Fraissard, Multinuclear high-resolution solid-state nuclear magnetic resonance studies of amorphous silica-aluminas, Appl. Catal. 77 (1991) 149–161.
[35] D. Fan, P. Tian, X. Su, Y. Yuan, D. Wang, C. Wang, M. Yang, L. Wang, S. Xu, Z. Liu, Aminothermal synthesis of CHA-type SAPO molecular sieves and their catalytic performance in methanol to olefins (MTO) reaction, J. Mater. Chem. 1 (2013) 14206–14213.
[36] R.L. Smith, S. Svelle, P. del Campo, T. Fuglerud, B. Arstad, A. Lind, S. Chavan, M. P. Attfield, D. Akporiaye, M.W. Anderson, CHA/AEI intergrowth materials as catalysts for the Methanol-to-Olefins process, Appl. Catal., A 505 (2015) 1–7.
[37] L. Xuan, X. Wang, Y. Zhu, Z. Li, Synthesis of low-silica SAPO-34 at lower hydrothermal temperature by additional pressure and its enhanced catalytic performance for methanol to olefin, Microporous Mesoporous Mater. 323 (2021) 111218–111223.
[38] P. Ferri, C.G. Li, R. Millan, J. Martinez-Triguero, M. Moliner, M. Boronat, A. Corma, Impact of zeolite framework composition and flexibility on methanol-to-olefins selectivity: confinement or diffusion? Angew. Chem., Int. Ed. 59 (2020) 19708–19715.
[39] J. Zhong, J. Han, Y. Wei, Z. Liu, Catalysts and shape selective catalysis in the methanol-to-olefin (MTO) reaction, J. Catal. 396 (2021) 23–31.